UC Irvine
UC Irvine Previously Published Works

Title

Relationships Between Tau and Glucose Metabolism Reflect Alzheimers Disease Pathology in Cognitively Normal Older Adults.

Permalink

https://escholarship.org/uc/item/8g1548ss

Journal

Cerebral Cortex, 29(5)

Authors

Adams, Jenna
Lockhart, Samuel
Li, Lexin
et al.

Publication Date

2019-05-01

DOI

10.1093/cercor/bhy078

Peer reviewed

ORIGINAL ARTICLE

Relationships Between Tau and Glucose Metabolism Reflect Alzheimer's Disease Pathology in Cognitively Normal Older Adults

Jenna N. Adams [1], Samuel N. Lockhart [1], Lexin Li[2] and William J. Jagust[1,3]

[1]Helen Wills Neuroscience Institute, University of California, Berkeley, CA 94720, USA, [2]Department of Biostatistics, University of California, Berkeley, CA 94720, USA and [3]Lawrence Berkeley National Laboratory, Berkeley, CA 94720, USA

Address correspondence to Jenna N. Adams, 132 Barker Hall MC #3190, University of California, Berkeley, CA 94720, USA. Email: jnadams@berkeley.edu orcid.org/0000-0002-6702-3851

Abstract

Tau is associated with hypometabolism in patients with Alzheimer's disease. In normal aging, the association between tau and glucose metabolism is not fully characterized. We used [^{18}F] AV-1451, [^{18}F] Fluorodeoxyglucose, and [^{11}C] Pittsburgh Compound-B (PiB) PET to measure associations between tau and glucose metabolism in cognitively normal older adults ($N = 49$). Participants were divided into amyloid-negative (PiB–, $n = 28$) and amyloid-positive (PiB+, $n = 21$) groups to determine effects of amyloid-β. We assessed both local and across-brain regional tau–glucose metabolism associations separately in PiB–/PiB+ groups using correlation matrices and sparse canonical correlations. Relationships between tau and glucose metabolism differed by amyloid status, and were primarily spatially distinct. In PiB– subjects, tau was associated with broad regions of increased glucose metabolism. In PiB+ subjects, medial temporal lobe tau was associated with widespread hypometabolism, while tau outside of the medial temporal lobe was associated with decreased and increased glucose metabolism. We further found that regions with earlier tau spread were associated with stronger negative correlations with glucose metabolism. Our findings indicate that in normal aging, low levels of tau are associated with a phase of increased metabolism, while high levels of tau in the presence of amyloid-β are associated with hypometabolism at downstream sites.

Key words: aging, Alzheimer's disease, amyloid-β, glucose metabolism, tau

Introduction

Alzheimer's disease (AD) is characterized by decreased cortical glucose metabolism, particularly in temporoparietal regions as measured in vivo with the positron emission tomography (PET) tracer [^{18}F] Fluorodeoxyglucose (FDG) (Minoshima et al. 1997). This hypometabolism is thought to reflect reduced synaptic activity (Rocher et al. 2003) consequent to neurodegenerative processes. PET studies initially sought to relate the reduced glucose metabolism to the presence of amyloid-β plaques, quantified using PET tracers such as [^{11}C] Pittsburgh Compound-B

(PiB). However, the spatial distribution of hypometabolism and amyloid-β plaques are largely distinct in both AD patients and amyloid-positive cognitively normal older adults (Li et al. 2008; Rabinovici et al. 2010; Furst et al. 2012; La Joie et al. 2012; Altmann et al. 2015). Additionally, small and inconsistent relationships between amyloid measures and glucose metabolism across studies add skepticism about whether amyloid-β is the driving force behind hypometabolism (Jagust and Landau 2012; Lowe et al. 2014; Oh et al. 2014; Altmann et al. 2015).

Emerging evidence suggests that the deposition of the hyper-phosphorylated tau protein may be associated with reduced glucose metabolism. When tau is hyperphosphorylated it dissociates from microtubules and accumulates in the somatodendritic compartment of the neuron, forming neurofibrillary tangles (NFTs), one of the hallmarks of AD pathology (Wang and Mandelkow 2015). The recent advent of PET tracers targeting tau NFTs, such as the tracer [18F] AV-1451 (Xia et al. 2013), has enabled the investigation of the effects of tau in vivo. In studies of AD patients, regions of increased AV-1451 binding are strongly associated with regions of decreased glucose metabolism (Bischof et al. 2016; Ossenkoppele et al. 2015, 2016). Together with evidence from recent work demonstrating that tau is associated with decreased gray matter volume (LaPoint et al. 2017), altered functional activity and connectivity (Marks et al. 2017; Schultz et al. 2017), and reduced cognitive function (Brier et al. 2016; Maass, Lockhart et al. 2017), it is likely that tau is a closer link than amyloid-β to the neurodegenerative processes in AD.

The association between tau deposition and glucose metabolism has not yet been extensively explored in cognitively normal older adults. Hyperphosphorylated tau is present in the medial temporal lobes of the majority of cognitively normal older adults, and then appears to spread to lateral temporal and limbic regions in the presymptomatic stages of AD (Braak and Braak 1991; Schöll et al. 2016). For this reason, investigating the relationship between early tau deposition and glucose metabolism in cognitively normal older adults is vital to understanding the onset of disease. While a recent study (Hanseeuw et al. 2017) found negative associations between AV-1451 and FDG in amyloid-positive cognitively normal older adults in specific brain regions, a full accounting of tau throughout the cortex is needed to better understand the effects of tau on glucose metabolism in aging and development of disease.

The current study investigated the association between tau and glucose metabolism in amyloid-negative and amyloid-positive cognitively normal older adults with AV-1451, FDG, and PiB PET. We examined tau–glucose metabolism associations with three separate hypotheses in regards to the presence of amyloid-β, local versus non-local effects, and the progression of tau spread. First, we hypothesized that the relationship between tau and glucose metabolism would differ in subjects with and without the presence of amyloid-β. As subjects with high levels of global amyloid-β may be on track for developing Alzheimer's disease, we expected to observe strong negative relationships between tau and glucose metabolism primarily within this population. We therefore examined amyloid-negative and amyloid-positive older adults separately to determine how the presence of global amyloid-β affects tau–glucose metabolism relationships.

Second, we hypothesized that associations between tau and glucose metabolism in a cognitively normal older adult sample would primarily be spatially distinct, rather than occurring locally. Because glucose metabolism reflects synaptic activity, and tau is deposited in the soma, changes in glucose metabolism due to tau deposition should be observed at downstream sites. However, previous studies in AD and normal aging have primarily investigated local associations (Bischof et al. 2016; Ossenkoppele et al. 2015, 2016; Hanseeuw et al. 2017). In older adults, the investigation of non-local associations has been limited to the effects of tau in the entorhinal cortex and inferior temporal lobe (Hanseeuw et al. 2017), although in this population tau deposition may already encompass additional temporal and limbic regions. To thoroughly investigate both local and non-local effects of tau, we used across-brain correlation

matrices and sparse canonical correlations to characterize the complex spatial relationships between tau and glucose metabolism across numerous cortical regions.

Finally, we hypothesized that the stage of presymptomatic progression, modeled as the extent of tau pathology in a region, could help explain the observed patterns of tau–glucose metabolism associations. We thus related both the order of tau spread and the amount of tau pathology to the strength and direction of tau–glucose metabolism correlations. The goal of this analysis was to provide a biological explanation for the complex pattern of correlations between tau and glucose metabolism, and assess whether the relationship between tau spread and glucose metabolism changes can help further elucidate the pathogenesis of Alzheimer's disease.

Materials and Methods

Participants

Forty-nine cognitively normal older adults from the Berkeley Aging Cohort Study (BACS) with [18F] AV-1451, [18F] Fluorodeoxyglucose (FDG), and [11C] Pittsburgh Compound-B (PiB) PET scans acquired within 1 year were included for analysis. Eligibility requirements for BACS participants include: age of ≥60 years; cognitively normal status (Mini-Mental State Examination score ≥25 and normal neuropsychological examination); no serious neurological, psychiatric, or medical illness; no major MRI or PET contraindications; and independent living in the community. The Institutional Review Boards of the University of California, Berkeley, and the Lawrence Berkeley National Laboratory approved the study, and all participants provided written informed consent.

Structural MRI Acquisition

Structural MRIs were used to guide PET region-of-interest (ROI) data analysis and were acquired on a 1.5 T Siemens Magnetom Avanto system (Siemens, Inc., Iselin, NJ, USA) at Lawrence Berkeley National Laboratory (LBNL). High resolution T1-weighted magnetization prepared rapid gradient echo (MPRAGE) scans were acquired for each participant (TR = 2110 ms, TE = 3.58 ms, FA = 15°, 1 × 1 × 1 mm resolution). In one subject, severe motion artifacts rendered the most recent 1.5 T T1 scan unusable, so a previous 1.5 T T1 scan with the same acquisition parameters was substituted for this subject's preprocessing and analyses. MRI scans were performed an average of 96 ± 145 days from AV-1451, 42 ± 116 days from FDG, and 45 ± 118 days from PiB.

PET Acquisition

All PET scans were acquired at LBNL. AV-1451 was synthesized at LBNL's Biomedical Isotope Facility with a protocol described previously (Schöll et al. 2016), and acquired on a BIOGRAPH PET/CT Truepoint 6 scanner (Siemens, Inc.). Participants underwent one of two acquisition schemes: full dynamic scans (n = 23; 0–100 min post-injection with 4 × 15, 8 × 30, 9 × 60 s, and 2 × 3, 16 × 5 min frames; and 120–150 min, 6 × 5 min frames), or scans acquired between 75 and 115 min post-injection (n = 26; 8 × 5 min frames). Data were analyzed from frames between 80 and 100 min for both acquisition schemes. FDG was supplied by a radiopharmacy (IBA Molecular), and acquired on either the BIOGRAPH scanner (n = 43) or on an ECAT EXACT HR scanner (Siemens, Inc.; n = 6). Six emission frames lasting 5 min each were acquired between 30 and 60 min post-injection. Participants had their eyes and ears unoccluded during tracer uptake. PiB was synthesized at LBNL's Biomedical Isotope Facility with a protocol

described previously ([Mathis et al. 2003](#)), using the same scanner for acquisition as for FDG. Thirty-five dynamic acquisition frames were acquired for 90 min post-injection (4 × 15, 8 × 30, 9 × 60, 2 × 180, 10 × 300, and 2 × 600 s).

For AV-1451, a CT scan was performed before the start of each emission acquisition. For PiB and FDG, either a 10-min transmission scan or a CT was obtained. Reconstruction of all PET images used an ordered subset expectation maximization algorithm, with attenuation correction, scatter correction, and smoothing using a 4 mm Gaussian kernel. AV-1451 was acquired an average of 84 ± 105 days from FDG, and 80 ± 108 days from PiB. FDG and PiB were often acquired on the same day, with an average interscan interval of 6 ± 12 days.

Structural MRI Processing

T1-weighted images were processed with FreeSurfer v5.3.0 (http://surfer.nmr.mgh.harvard.edu/) to derive anatomical ROI masks in native space. Segmentations were manually checked to ensure accuracy. Specific ROIs were extracted and used for PET reference regions, global PiB values, and for AV-1451/FDG regional analyses. ROIs were also used for partial volume correction for the AV-1451 and FDG data.

PET Processing

AV-1451 images were realigned, averaged, and coregistered to the subject's MRI using Statistical Parametric Mapping 12 (SPM12, www.fil.ion.ucl.ac.uk/spm). Standardized uptake value (SUV) images were calculated based on mean tracer uptake over the 80–100 min averaged data. SUV images were normalized by an inferior cerebellar gray reference region ([Baker et al. 2017](#)) to create SUV ratio (SUVR) images in native space. Mean SUVR values were calculated for ROIs derived from FreeSurfer segmentation of the subject's MRI and used for subsequent analyses. In addition, partial volume correction was applied using a modified Geometric Transfer Matrix approach ([Rousset et al. 1998](#)) as described in [Baker et al. (2017)](#), and analyses were repeated using these data (shown in Supplementary Material).

FDG images were realigned, averaged, and coregistered to the subject's MRI using SPM12. SUV images were calculated based on mean tracer uptake over 30–60 min post-injection. SUV images were normalized by a pons reference region, which was created by manually editing each subject's native space brainstem segmentation produced by FreeSurfer. Mean SUVR values were calculated for native space FreeSurfer ROIs and used for subsequent analyses. Partial volume correction was also applied using a method similar to that used for AV-1451, and analyses were repeated using these data (shown in Supplementary Material).

PiB images were realigned, averaged across frames from the first 20 min of acquisition, and used for coregistration to the subject's MRI using SPM12. Distribution volume ration (DVR) images were calculated using Logan graphical analysis (35–60 min post-injection) and a whole cerebellar gray reference region ([Logan 2000](#); [Price et al. 2005](#)). A measure of global PiB uptake was calculated using cortical FreeSurfer ROIs as previously described ([Mormino et al. 2011](#)). A threshold of 1.065 was applied to the global PiB DVR to determine amyloid positivity, and subjects were dichotomized into amyloid-negative (PiB–) and amyloid-positive (PiB+) groups.

Region of Interest Selection

To investigate regions from stages 1–4 of the Braak neuropathological grading scheme for tau deposition ([Braak and Braak 1991](#)), we assessed AV-1451 in 26 FreeSurfer ROIs across both hemispheres. We did not include Braak 5–6 regions because a cognitively normal older adult sample is unlikely to demonstrate AV-1451 binding in these regions ([Maass, Landau et al. 2017](#)). AV-1451 ROIs included the medial temporal lobe (entorhinal, hippocampus, parahippocampal gyrus, amygdala, fusiform, and lingual gyrus), temporal lobe (inferior and middle temporal gyrus), cingulate (rostral anterior, caudal anterior, posterior, and isthmus cingulate or retrosplenial cortex), and insula.

FDG ROIs included all ROIs for AV-1451, plus additional ROIs from Braak 5 regions. We included Braak 5 regions to determine if tau could have associations with glucose metabolism in downstream regions prior to the spread to that region. FDG included additional ROIs in the temporal lobe (superior temporal gyrus and banks of the superior temporal sulcus), parietal lobe (precuneus, inferior, superior, and supramarginal gyrus), frontal lobe (superior frontal, orbitofrontal [composite of medial orbitofrontal, lateral orbitofrontal, and frontal pole], midfrontal [composite of rostral middle frontal and caudal middle frontal], and parsfrontal [composite of pars opercularis, pars orbitalis, and pars triangularis]), and lateral occipital cortex.

Statistical Analysis

Demographic Data and Across-Brain Correlations. To assess demographic differences between PiB– and PiB+ subjects, categorical variables were analyzed using Chi-squared tests, while continuous variables were analyzed using independent samples t-tests. For the across-brain correlation analysis, Pearson partial correlations controlling for age and sex were performed between all combinations of AV-1451 ROIs (26 ROIs) and FDG ROIs (48 ROIs). Due to the large number of statistical tests, a permutation approach was applied to assess significance. Each correlation pair was permuted 10 000 times, and adjusted P-values of <0.05 were considered significant. All statistical analyses for demographic data and across-brain correlations were performed with MATLAB version 2015a (The MathWorks, Inc., Natick, MA, USA).

Sparse Canonical Correlation Analysis. To assess multivariate relationships between AV-1451 and FDG, a sparse canonical correlation was performed. Canonical correlation analysis identifies a linear combination of variables in one modality that is maximally correlated with a linear combination of variables in a second modality ([Hotelling 1936](#); [Härdle and Simar 2007](#)). In each modality, every variable is assigned a weight that represents its contribution to the maximized correlation. The original variables are then multiplied by these weights to produce a multivariate projection in each modality, which are then correlated to compute the canonical correlation. Multiple canonical correlations can be calculated by using the residual data of the canonical variates to compute the subsequent canonical correlation. Sparse canonical correlation extends on the usual canonical correlation by imposing a sparsity penalty onto the canonical variates ([Witten et al. 2009](#)). This sparsity penalty limits the number of variables that contribute to the correlation by reducing the lowest weightings to zero. Sparse canonical correlation therefore finds the most meaningful variables in each modality that highly correlate with variables in the other modality.

Sparse canonical correlation analysis (SCCA) was performed using the Penalized Multivariate Analysis (PMA) R package (Witten et al. 2009), implemented in R version 3.3.2 (http://www.r-project.org/). Bilateral AV-1451 and FDG ROIs were chosen for analysis to reduce redundancy in the multivariate model. Effects of age and sex were removed from the bilateral AV-1451 and FDG data by calculating the residuals, which were used for analyses. To focus on the most meaningful ROIs, a lasso penalty of 0.5 was applied to both the AV-1451 and FDG data to achieve a suitable level of sparsity. To make the interpretation of the weights more clear, AV-1451 weights were constrained to be positive, while FDG weights were not constrained. These constraint parameters allow the weights to be interpreted as "an increase in AV-1451 is associated with an increase/decrease in FDG". Finally, all data were mean centered and scaled. The first three significant canonical correlation dimensions of each group (PiB–/PiB+) were selected for interpretation. Significance was determined by correlating the multivariate projections of AV-1451 and FDG, which produces a correlation coefficient for each dimension and an associated P-value. P-values of <0.05 were considered significant.

Quantifying the Order of Tau Spread. We were interested in determining whether brain regions affected earlier in the phase of tau deposition had different effects on glucose metabolism than brain regions affected later. We therefore modeled the order of tau spread within PiB– and PiB+ subjects using a method previously reported by Cho et al. (2016). First, we identified a low pathology reference group of subjects from our sample that would be used to compute z-scores. Subjects needed to meet two criteria for inclusion into the reference group: (1) amyloid-negative status (global PiB < 1.065); (2) bilateral entorhinal AV-1451 SUVR < 1.2. Next, all subjects' bilateral AV-1451 data were z-scored based on the reference group. Within each subject, if an ROI's AV-1451 z-score was >2.5, the ROI was classified as being tau positive. Within the PiB– and PiB+ groups separately, and for each ROI, we then calculated the percentage of subjects that had a tau positive ROI ("percent positivity"). Finally, to determine the spreading pattern of tau within each group, ROIs were ranked by the percentage of tau positivity, and ties were resolved by ranking the ROI with the highest mean z-score first.

Extent of Tau Pathology and AV-1451–FDG Correlations. In order to model how the progression of tau pathology was related to the pattern of glucose metabolism, we determined how the spreading order of AV-1451 and the amount of AV-1451 in an ROI related to the direction and strength of AV-1451–FDG correlations. We correlated the order of spread and mean SUVR of each AV-1451 ROI with its range of FDG correlation coefficients (computed from the across-brain analyses). Pearson's r correlation coefficients for each AV-1451–FDG pair were first transformed into Fisher's z' to obtain a normally distributed variable. Due to the ordinal nature of the AV-1451 spread index, Spearman correlations were performed between AV-1451 spreading order and each AV-1451 ROI's range of Fisher's z' transformed correlation coefficients (including both right and left hemisphere correlations). Pearson correlations were performed between the mean AV-1451 SUVR in each ROI, and each AV-1451 ROI's range of Fisher's z' transformed correlation coefficients. These correlations were performed separately in the PiB– and PiB+ groups.

Results

Sample Characteristics

Demographic information and group differences for the PiB– and PiB+ groups are presented in Table 1. Of the 49 subjects, 28 subjects were classified as PiB–, and 21 subjects were classified as PiB+. There was no significant group difference in age, sex, education, or time between AV-1451 and FDG scan acquisition (all Ps > 0.05). By design, the PiB+ group had higher global PiB values than the PiB– group (t = –6.81, P < 0.001). In addition, the PiB+ group had a higher prevalence of APOE ε4 positivity (X^2 = 20.57, P < 0.001), and a slightly lower MMSE score (t = 2.18, P = 0.03).

AV-1451–FDG Across-Brain Correlations

Within the PiB– and PiB+ groups separately, Pearson partial correlations controlling for age and sex were performed for each AV-1451–FDG pair of ROIs (Fig. 1). Significance, determined by permutation testing, reflects adjusted P-values.
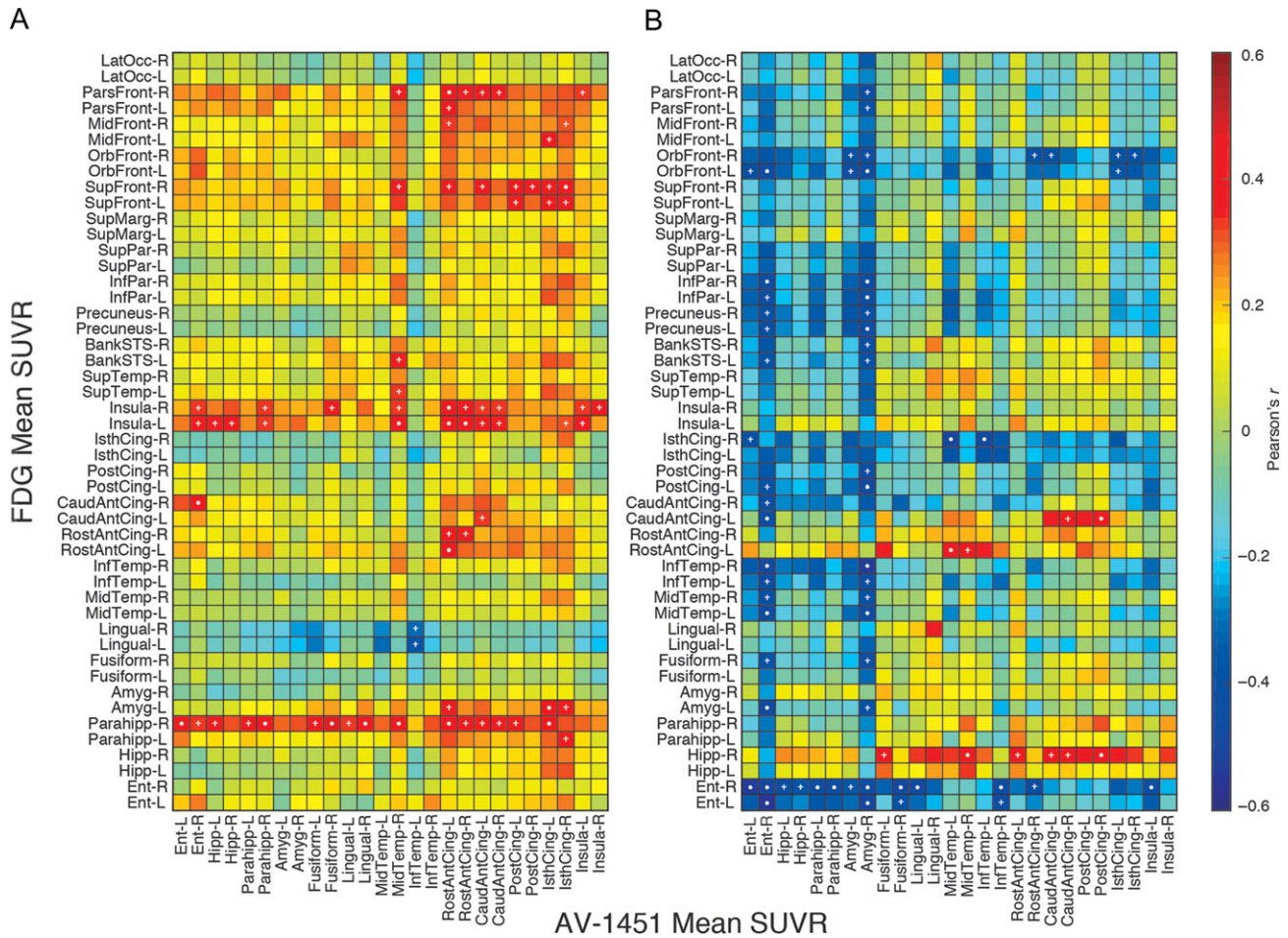
In the PiB– group, correlations between AV-1451 and FDG were predominantly positive (Fig. 1A), reflecting overall increases in AV-1451 associated with increases in FDG. There were especially strong positive correlations between AV-1451 throughout the brain and increases in FDG in both the parahippocampal gyrus and insula. Additionally, strong positive correlations were observed between AV-1451 in cingulate regions (rostral anterior, caudal anterior, posterior, and isthmus), and FDG in frontal regions (superior frontal, orbitofrontal, midfrontal, and parsfrontal). Moderate negative correlations were observed between AV-1451 of the inferior and middle temporal gyrus and FDG of the lingual gyrus.

In contrast, correlations between AV-1451 and FDG in the PiB+ group were predominantly negative (Fig. 1B). The positive relationships between AV-1451 and FDG in parahippocampal gyrus and insula found in the PiB– group weakened or became negative. Conversely, AV-1451 throughout the brain was associated with strong negative correlations with FDG in bilateral entorhinal cortex, isthmus cingulate cortex, and orbitofrontal cortex. AV-1451 in the medial temporal lobe, particularly in the entorhinal cortex and amygdala, was associated with strong negative correlations

Table 1. Demographics of the PiB– and PiB+ groups

	PiB– (n = 28) M (SD) or n (%)	PiB+ (n = 21) M (SD) or n (%)	t or X^2	P
Age (years)	78.9 (6.8)	78.1 (3.6)	0.56	0.58
Sex (female)	18 (64%)	14 (67%)	0.03	0.86
Education (years)	16.9 (1.8)	16.0 (2.1)	1.66	0.10
APOE ε4 (+)	3 (11%)	15 (75%)[a]	20.57	<0.001
MMSE	29.1 (1.0)	28.3 (1.4)	2.18	0.03
Global PiB	1.01 (0.03)	1.37 (0.24)	–6.81	<0.001
AV-1451–FDG scan acquisition time difference (days)	93 (122)	73 (79)	0.69	0.49

PiB–, amyloid-β negative older adults; PiB+, amyloid-β positive older adults; APOE, apolipoprotein E; MMSE, Mini-Mental State Examination. [a]One PiB+ subject missing APOE data.

Figure 1. Across-brain AV-1451–FDG correlations. Pearson partial correlations between AV-1451 and FDG ROIs in the PiB– (A) and PiB+ (B) groups. Adjusted P-values were computed from a permutation analysis, with a white dot in each cell indicating adjusted P < 0.05, and a white plus (+) indicating adjusted P < 0.10. Ent, Entorhinal Cortex; Hipp, Hippocampus; Parahipp, Parahippocampal Gyrus; Amyg, Amygdala; Mid, Middle; Temp, Temporal; Inf, Inferior; Rost, Rostral; Ant, Anterior; Cing, Cingulate; Caud, Caudal; Post, Posterior; Isth, Isthmus; Sup, Superior; BankSTS, Banks of the Superior Temporal Sulcus; Par, Parietal; Marg, Marginal; Front, Frontal; Orb, Orbital; Lat, Lateral; Occ, Occipital.

spanning the majority of FDG ROIs. The strongest negative associations of AV-1451 in entorhinal cortex and amygdala were with FDG in the middle and inferior temporal gyrus, posterior and isthmus cingulate cortex, precuneus, inferior parietal lobe, and the orbitofrontal cortex. Positive associations between AV-1451 and FDG were also observed in the PiB+ group, though to a lesser extent than negative correlations. Positive correlations were mostly associated with AV-1451 outside of the medial temporal lobe. For example, AV-1451 of lateral temporal and cingulate regions were positively associated with FDG of the hippocampus, rostral anterior cingulate, and caudal anterior cingulate cortex.

The across-brain correlation analysis was repeated with partial volume corrected AV-1451 and FDG data (Supplementary Fig. 1). Directly comparing the results with and without PVC, the correlation values obtained in each analysis were highly correlated (PiB–, $r = 0.62$, P < 0.001; PiB+, $r = 0.74$, P < 0.001). In addition, no correlation strengths were significantly different after PVC (all Ps > 0.05), as determined by comparing each correlation value before and after PVC with Fisher's z' tests. However, there were still nonsignificant changes and qualitative differences between the matrices. For example, the strength of positive correlations tended to increase in both groups after partial volume correction. Also, more

negative correlations were revealed in the PiB– group in association with medial temporal lobe tau and in the lingual gyrus.

Sparse Canonical Correlation Analysis

PiB– SCCA Results

To extract meaningful patterns from the correlation matrices in a data-driven manner, a sparse canonical correlation analysis (SCCA) was performed. See Figure 2A–C for a visual representation of the PiB– SCCA results, and Table 2 for the weights of each region that contributed to the dimension. In the PiB– group, Dimension 1 was represented by positive AV-1451 weights in the cingulate cortex, and positive FDG weights in the frontal and medial temporal lobes (Fig. 2A; $r = 0.38$, P = 0.045). AV-1451 had the strongest positive weights in the rostral anterior cingulate cortex, with the isthmus, caudal anterior, and posterior cingulate cortices also contributing positive weight. The strongest positive FDG weights included the parahippocampal gyrus, insula, and pars frontal cortex. The superior frontal, mid frontal, and rostral anterior cingulate cortex also demonstrated positive weights.

Dimension 2 was represented by positive AV-1451 weights primarily in the temporal lobe, and both positive and negative
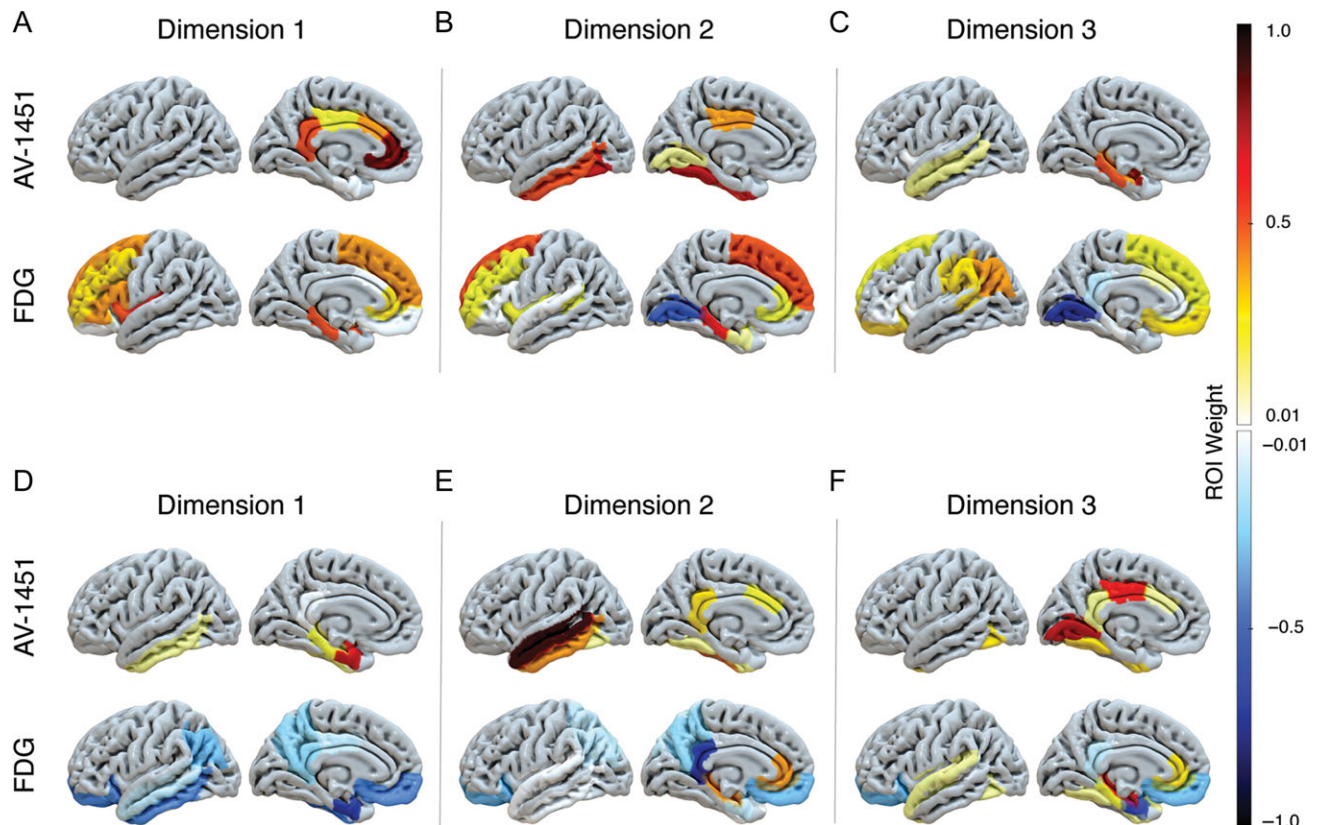
Figure 2. Sparse canonical correlation analysis. Significant dimensions produced from the sparse canonical correlation analysis in the PiB− (A–C) and PiB+ (D–F) groups. Dimensions represent maximized correlations between sparse weightings of AV-1451 and FDG ROIs. Each dimension consists of AV-1451 weights, representing an increase (positive weights) in AV-1451, with the corresponding FDG weights, representing either an increase or decrease (negative weights) in FDG. Weights reduced to zero due to sparsity constraints are not included in the color scale. Bilateral ROIs are depicted on a left hemisphere template brain.

FDG weights in the frontal and temporal cortices (Fig. 2B; $r =$ 0.44, P = 0.02). AV-1451 had the strongest positive weight in the fusiform gyrus, with the inferior temporal gyrus, posterior cingulate cortex, and lingual gyrus also demonstrating positive weights. FDG was represented by positive weights in the parahippocampal gyrus and superior frontal cortex, among other frontal and temporal regions. FDG was also represented by a negative weight in the lingual gyrus.

Dimension 3 was represented by positive AV-1451 weights primarily in the medial temporal lobe, and both positive and negative FDG weights in widespread cortical regions (Fig. 2C; $r = 0.39$, P = 0.04). AV-1451 had the strongest positive weights in the amygdala, parahippocampal gyrus, and hippocampus. FDG had strong positive weights in the inferior parietal lobe, banks of the superior temporal sulcus, and orbitofrontal cortex. FDG had negative weights in the lingual gyrus and isthmus cingulate cortex.

Replicating the analysis with partial volume corrected (PVC) data obtained largely consistent results (Supplementary Fig. 2). Two dimensions in the PVC analysis passed the significance threshold (Dimension 1, $r = 0.44$, P = 0.02; Dimension 2, $r = 0.63$, P < 0.001). AV-1451 weights from the two PVC dimensions resembled AV-1451 weights in the non-PVC dimensions. FDG weights in the PVC dimensions included some new negative weights, in addition to positive weights similar to those observed in the non-PVC data.

PiB+ SCCA Results

See Figure 2D–F for a visual representation of the PiB+ SCCA results, and Table 3 for the weights of each region that contributed to the dimension. In the PiB+ group, Dimension 1 was represented by positive AV-1451 weights primarily in the medial temporal lobe, and negative FDG weights throughout the cortex (Fig. 2D; $r = 0.50$, P = 0.02). AV-1451 had the strongest positive weights in the entorhinal cortex, amygdala, and the parahippocampal gyrus. FDG had the strongest negative weights in the entorhinal cortex, orbitofrontal cortex, and inferior temporal gyrus. The precuneus, inferior parietal, isthmus cingulate, and posterior cingulate also demonstrated strong negative weights.

Dimension 2 was represented by positive AV-1451 weights in the lateral temporal lobe and cingulate cortex, and both negative and positive FDG weights throughout the cortex (Fig. 2E; $r = 0.60$, P = 0.004). AV-1451 had the strongest positive weights in the middle and inferior temporal gyrus, and in the isthmus and caudal anterior cingulate cortex. FDG had strong negative weights in the isthmus cingulate cortex, orbitofrontal cortex, precuneus, and inferior parietal cortex. FDG had positive weights in the rostral anterior cingulate and hippocampus.

Dimension 3 was represented by positive AV-1451 weights in the cingulate and temporal lobes, and both negative and positive FDG weights throughout the cortex (Fig. 2F; $r = 0.77$, P < 0.001). AV-1451 had the strongest positive weights in the lingual gyrus, fusiform gyrus, and posterior cingulate cortex. FDG had strong negative weights in the entorhinal cortex, orbitofrontal cortex, and isthmus cingulate cortex. FDG had a strong positive weight in the hippocampus, with moderate positive

Table 2 AV-1451 and FDG weights for each region of interest in the PiB– sparse canonical correlation analysis

ROI	Dimension 1 Weights		Dimension 2 Weights		Dimension 3 Weights	
	AV-1451	FDG	AV-1451	FDG	AV-1451	FDG
Entorhinal	0.01	0	0	0.09	0	0
Hippocampus	0	0	0	0	0.38	0
Parahippocampal	0	0.53	0	0.62	0.47	0.03
Amygdala	0	0	0	0	0.79	0
Fusiform	0	0	0.73	0	0	0
Lingual	0	0	0.12	−0.52	0	−0.71
Mid Temporal	0	0	0	0	0.14	0
Inf Temporal	0	0	0.52	0	0	0
Rost Ant Cingulate	0.77	0.29	0	0.16	0	0
Caud Ant Cingulate	0.37	0.04	0	0	0	0.06
Post Cingulate	0.16	0	0.43	0	0	0
Isth Cingulate	0.50	0	0	0	0	−0.13
Insula	0	0.50	0	0.16	0.03	0.01
Sup Temporal	—	0	—	0.03	—	0
BankSTS	—	0	—	0.20	—	0.35
Precuneus	—	0	—	0	—	0
Inf Parietal	—	0	—	0	—	0.42
Sup Parietal	—	0	—	0	—	0
Sup Marginal	—	0	—	0	—	0.25
Sup Frontal	—	0.37	—	0.47	—	0.19
Orb Frontal	—	0.04	—	0	—	0.28
Mid Frontal	—	0.27	—	0.16	—	0
Pars Frontal	—	0.42	—	0.05	—	0.01
Lat Occipital	—	0	—	0	—	0

ROI, region of interest; Mid, middle; Inf, inferior; Rost, rostral; Ant, anterior; Caud, caudal; Post, posterior; Isth, isthmus; Sup, superior; BankSTS, bank of superior temporal sulcus; Orb, orbital; Lat, lateral.

weights in the rostral anterior cingulate cortex, parahippocampal gyrus, fusiform gyrus, and superior temporal gyrus.

Replicating the analysis with partial volume corrected data generated comparable results (Supplementary Fig. 2). Dimension 1 of the PVC data ($r = 0.54$, $P = 0.01$) represented very similar AV-1451 positive weights and FDG negative weights as Dimension 1 of the non-PVC data, with the addition of new FDG positive weights. Dimension 2 of the PVC data ($r = 0.61$, $P = 0.003$) closely resembled Dimension 3 of the non-PVC data, with additional positive weights in the FDG dimension. Dimension 3 of the PVC data ($r = 0.85$, $P < 0.001$) was nearly identical to Dimension 2 of the non-PVC data, with weights slightly shifted across the two analyses.

Extent of Tau Pathology and AV-1451–FDG Correlations

We next sought to determine how the strength and direction of AV-1451–FDG correlations related to the extent of tau pathology in an ROI. We speculated that relating these correlation coefficients to the order of tau spread in the brain, and to the amount of AV-1451 in a region, would help clarify the complex patterns of correlations observed in both the correlation matrices and the SCCA results.

Tau Spread & AV-1451–FDG Correlations

Of the 49 subjects included in this study, 22 met criteria for the low pathology reference group. All subjects' bilateral AV-1451 data were then z-scored based on this reference group, and indices of tau spread were calculated in PiB– and PiB+ groups separately. ROIs were ranked by the group metrics of percent positivity, and then by mean z-score. Results of the tau spread ranking are shown in Table 4. Although there were slight differences, the overall ranking reflected a high proportion of cases with pathology in the medial temporal lobe, with subsequent involvement of isthmus cingulate (retrosplenial cortex), lateral temporal lobe, and anterior cingulate cortex. In the PiB– group, only one subject demonstrated "positive" tau ROIs outside of the medial temporal lobe, thus the ranking is primarily based on the mean z-score of each region rather than "percent positivity". Although we recognize that this model is based on cross-sectional data, we refer to these patterns as reflective of tau spread through the brain.

Associations between the order of AV-1451 spread and the Fisher's z' transformed AV-1451–FDG correlation coefficients are presented in Figure 3A. In the PiB– group, there was a weak positive correlation between AV-1451 spreading order and the range of correlation coefficients ($r_s = 0.06$, $P = 0.04$). Regions to which AV-1451 spread first demonstrated weak positive correlations with FDG, while later regions of AV-1451 spread had stronger positive correlations with FDG. In the PiB+ group, there was a positive correlation between AV-1451 spreading order and the range of correlation coefficients ($r_s = 0.36$, $P < 0.001$). Regions to which AV-1451 spread first demonstrated strong negative correlations with FDG, while later regions of AV-1451 spread had weaker negative correlations with FDG.

Mean SUVR & AV-1451–FDG Correlations

Associations between the mean AV-1451 SUVR of each ROI and the Fisher's z' transformed AV-1451–FDG correlation coefficients are presented in Figure 3B. In the PiB– group, there was a negative correlation between mean AV-1451 SUVR and the range of correlation coefficients ($r = -0.22$, $P < 0.001$). As the mean AV-1451 SUVR of an ROI increased, the range of correlation coefficients became less positive. In the PiB+ group, there was also a negative correlation between mean AV-1451 SUVR and the range of correlation coefficients ($r = -0.27$, $P < 0.001$). As the mean AV-1451 SUVR of an ROI increased, the range of correlation coefficients became more negative.

To determine if PiB group status had an effect on the range of correlation coefficients over and above mean AV-1451 SUVR, a one-way analysis of covariance (ANCOVA) was performed. Mean AV-1451 SUVR was the predictor, Fisher's z' transformed correlation coefficients were the dependent variable, and PiB status was entered as the grouping variable. ANCOVA results revealed a significant effect of PiB status on the range of correlation coefficients after controlling for the effects of mean AV-1451 SUVR ($F(1, 2492) = 233.92$, $P < 0.001$). There was no interaction between PiB group status and mean AV-1451 SUVR on the range of correlation coefficients ($F(1, 2492) = 1.94$, $P = 0.16$). These results indicate that while increasing mean AV-1451 is associated with a similar decrease in AV-1451–FDG correlations in both groups, the presence of amyloid-β in the PiB+ group exerts a negative effect on correlations over and above AV-1451 alone.

Discussion

The current study investigated the association between tau and glucose metabolism across numerous cortical regions within cognitively normal older adults. We found complex spatial relationships between tau and glucose metabolism that depended on global amyloid-β status and the extent of tau

Table 3 AV-1451 and FDG weights for each region of interest in the PiB+ sparse canonical correlation analysis.

ROI	Dimension 1 Weights		Dimension 2 Weights		Dimension 3 Weights	
	AV-1451	FDG	AV-1451	FDG	AV-1451	FDG
Entorhinal	0.73	−0.68	0	−0.07	0	−0.64
Hippocampus	0.08	0	0	0.42	0	0.56
Parahippocampal	0.18	0	0	0	0	0.23
Amygdala	0.63	0	0	0	0	0
Fusiform	0	0	0.08	0	0.28	0.15
Lingual	0	0	0	0	0.72	0
Mid Temporal	0	−0.09	0.86	0	0	0
Inf Temporal	0.13	−0.37	0.36	−0.05	0	0
Rost Ant Cingulate	0	0	0	0.44	0	0.29
Caud Ant Cingulate	0	0	0.24	0	0.12	0
Post Cingulate	0	−0.13	0	0	0.63	0
Isth Cingulate	0.05	−0.20	0.26	−0.65	0.06	−0.14
Insula	0	0	0	0	0	0
Sup Temporal	—	0	—	0.01	—	0.13
BankSTS	—	0	—	0	—	0.04
Precuneus	—	−0.24	—	−0.21	—	0
Inf Parietal	—	−0.31	—	−0.15	—	0
Sup Parietal	—	0	—	−0.11	—	0
Sup Marginal	—	0	—	0	—	0
Sup Frontal	—	0	—	0	—	0
Orb Frontal	—	−0.42	—	−0.34	—	−0.27
Mid Frontal	—	0	—	0	—	0
Pars Frontal	—	0	—	0	—	0
Lat Occipital	—	0	—	0	—	0

ROI, region of interest; Mid, middle; Inf, inferior; Rost, rostral; Ant, anterior; Caud, caudal; Post, posterior; Isth, isthmus; Sup, superior; BankSTS, bank of superior temporal sulcus; Orb, orbital; Lat, lateral.

pathology. In accordance with our first hypothesis, we found that the presence of global amyloid-β affected tau–glucose metabolism associations. In amyloid-negative subjects, tau across many cortical regions was associated with an increase in glucose metabolism. In contrast, in amyloid-positive subjects, tau in the medial temporal lobe was associated with widespread hypometabolism, while tau outside of the medial temporal lobe was associated with more complex patterns of both decreased and increased glucose metabolism. In relation to our second hypothesis, we found the relationship between tau and glucose metabolism to be largely spatially distinct, possibly reflecting remote effects of tau deposition on synaptic activity. With regard to our third hypothesis, we demonstrated that the extent of tau pathology corresponded to the association between tau and glucose metabolism. Regions with earlier tau spread and higher amounts of tau deposition had stronger negative associations with glucose metabolism, particularly in the amyloid-positive group. Together, these results suggest that low levels of tau pathology are associated with hypermetabolism. As tau continues to deposit, or as amyloid-β pathology interacts with tau, hypometabolism occurs. Furthermore, the spatial pattern of these relationships may offer insights about the spatiotemporal pattern of tau-related neurodegeneration.

Distinct Stages of Tau–Glucose Metabolism Associations

Our across-brain regional correlation analysis and multivariate sparse canonical correlations were in agreement in revealing differing associations between tau and glucose metabolism in amyloid-negative and amyloid-positive subjects. The strongest positive relationships in the amyloid-negative group showed high tau in the cingulate cortex associated with increased metabolism in the frontal lobe. The parahippocampal gyrus and insula also demonstrated increased metabolism in association with tau across many cortical regions. In the amyloid-positive group, increases of tau in the entorhinal cortex and amygdala were associated with widespread cortical hypometabolism. Outside of the medial temporal lobe, increasing tau in areas such as the inferior and middle temporal gyrus was largely associated with decreased glucose metabolism. These results are both consistent with and expand upon the findings of Hanseeuw et al. (2017), who found small positive correlations in amyloid-negative subjects, and negative associations between entorhinal and inferior temporal tau with cortical glucose metabolism in amyloid-positive subjects.

We hypothesized that this complex pattern of tau–glucose metabolism associations both within and across amyloid groups would be related to the extent of tau pathology in a region. After modeling the spreading order of tau within each group, we found that earlier regions of tau spread in the amyloid-positive group were associated with stronger negative correlations with glucose metabolism. Later regions of tau spread in the amyloid-negative group were associated with stronger positive associations between tau and glucose metabolism, though this ranking included regions of minimal tau binding. We also found that the presence of amyloid-β exerts a negative effect on tau–glucose metabolism correlations over and above the effects of tau alone, suggesting increased toxicity of the simultaneous presence of tau and amyloid-β. Together, our results support a model in which low levels of tau in the absence of amyloid-β are initially associated with increased glucose metabolism, possibly representing normal aging processes. Tau deposition in earlier affected regions and in the presence of amyloid-β deposits is

Table 4 Spreading order of AV-1451 in PiB− and PiB+ groups

Order	ROI	% Positivity	Z-score	SUVR
		PiB− (n = 28)		
1	Amygdala	10.7	0.53	1.21
2	Entorhinal Cortex	10.7	0.51	1.13
3	Hippocampus	7.1	0.41	1.23
4	Parahippocampal Gyrus	3.6	0.36	1.09
5	Insula	3.6	0.34	1.12
6	Caudal Anterior Cingulate	3.6	0.30	1.07
7	Isthmus Cingulate	3.6	0.30	1.10
8	Rostral Anterior Cingulate	3.6	0.28	1.09
9	Posterior Cingulate	3.6	0.27	1.14
10	Inferior Temporal Gyrus	0.0	0.26	1.14
11	Fusiform Gyrus	0.0	0.20	1.16
12	Middle Temporal Gyrus	0.0	0.19	1.15
13	Lingual Gyrus	0.0	0.16	1.10
		PiB+ (n = 21)		
1	Entorhinal Cortex	33.3	1.80	1.23
2	Amygdala	28.6	1.75	1.33
3	Parahippocampal Gyrus	28.6	1.55	1.19
4	Fusiform Gyrus	23.8	1.56	1.25
5	Inferior Temporal Gyrus	19.0	1.61	1.25
6	Hippocampus	19.0	1.23	1.33
7	Posterior Cingulate	19.0	1.19	1.22
8	Caudal Anterior Cingulate	19.0	1.13	1.14
9	Middle Temporal Gyrus	14.3	1.51	1.26
10	Isthmus Cingulate	14.3	1.22	1.17
11	Insula	14.3	1.11	1.19
12	Rostral Anterior Cingulate	4.8	0.93	1.16
13	Lingual Gyrus	4.8	0.61	1.13

ROI, region of interest; % Positivity, percentage of subjects crossing threshold for AV-1451 positivity; SUVR, standardized uptake value ratio.

associated with decreased glucose metabolism, presumably indicating the onset of neurodegeneration.

The directionality of the association between increased glucose metabolism and early tau deposition is unclear. Tau could provoke metabolic increases as a result of compensation (Ossenkoppele et al. 2014), tau-incited neuroinflammation (Heneka et al. 2015; Brendel et al. 2016), or hyperexcitability (Ong et al. 2013). Alternatively, increased glucose metabolism may drive initial tau propagation and spread. Neuronal activity has been shown to increase tau pathology and neuronal release (Wu et al. 2016). Increased metabolism related to subthreshold levels of amyloid-β (Hanseeuw et al. 2017) or APOE ε4 positivity (Yi et al. 2014) could thereby facilitate tau pathology, though this seems less likely to occur in our sample due to their low occurrence of APOE ε4 positivity. Finally, it is possible that tau deposition in the amyloid-negative group could be partly explained by off-target binding of the AV-1451 tracer.

The interpretation of how the positive relationship between tau and glucose metabolism may evolve is dependent on the mechanisms and reasons behind the tau deposition. For example, in the amyloid-negative group, tau deposition could be due to a normal aging process. It is possible that tau deposition in this group will remain low, and thus hypermetabolism may persist with limited consequences. However, even cognitively normal older adults with no evidence of amyloid pathology may experience high levels of tau deposition, especially in medial temporal lobe regions (Braak and Braak 1997). Similarly, if a subset of our subjects are in the precursor stages to AD or an evolving primary age-related tauopathy (PART) (Crary et al. 2014), then their tau deposition is likely to increase as well. It is

also possible that in some of our amyloid-negative subjects that as tau pathology increases in intensity and ultimately reaches a certain level, tau-related metabolic increases may yield to metabolic decline. We see signs of this decline in our amyloid-negative group in the PVC correlation matrices (see Supplementary Fig. 1A) and both the non-PVC and PVC SCCA (see Fig. 2C and Supplementary Fig. 2A), where medial temporal lobe tau, which demonstrates the highest deposition, is associated with decreased temporal and posterior cingulate glucose metabolism. Without longitudinal analyses, it is hard to determine how the relationship between tau and hypermetabolism will progress.

In regions of high tau deposition and in the presence of amyloid-β, tau demonstrated negative associations with glucose metabolism. The interaction between tau and amyloid-β has been shown to increase toxicity to neurons (Wang and Mandelkow 2015), leading to neurodegeneration and thus hypometabolism. This is consistent with the theorized progression of tau and amyloid-β pathology in cognitively normal older adults developing into AD. Alternatively, it is possible that hypometabolism in amyloid-positive subjects could precede tau deposition. For example, downstream mechanisms related to decreased glucose metabolism have been found to induce tau hyperphosphorylation (Planel et al. 2004). While there are numerous prior reports of reductions in glucose metabolism in aging, these findings are typically accentuated in prefrontal cortex and do not recapitulate the typical pattern seen in AD (represented in Fig. 2D) (Zuendorf et al. 2003; Shen et al. 2012). Nevertheless, drawing firm causal inferences from these data will require longitudinal observations.
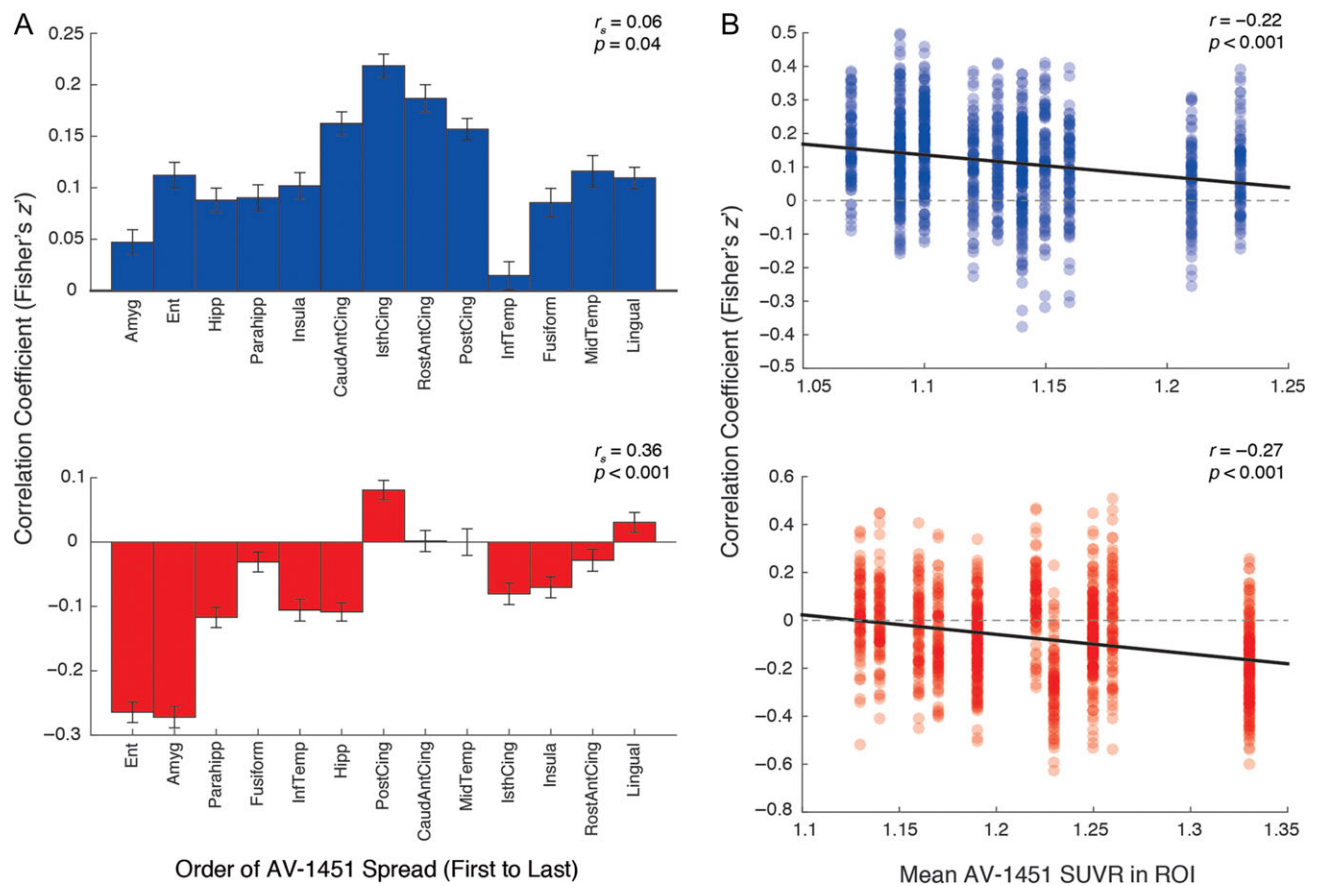
Figure 3. Extent of Tau pathology and AV-1451–FDG correlations. The relationship between the order of tau spread and the range of AV-1451–FDG correlation coefficients is depicted as a bar plot in (A). AV-1451 ROIs are ranked by the order of tau spread from first to last in the PiB– (top) and PiB+ (bottom) groups separately. Bar graphs represent the mean Fisher's z' transformed correlation coefficient (± standard error) for each AV-1451–FDG pair associated with the corresponding AV-1451 ROI. The relationship between mean AV-1451 SUVR and the range of AV-1451–FDG correlation coefficients is depicted as a scatter plot in (B) for the PiB– (top) and PiB+ (bottom) groups separately. The mean SUVR of each AV-1451 ROI is plotted on the x-axis. Each individual Fisher's z' transformed correlation coefficient value is plotted corresponding with the mean SUVR of the AV-1451 ROI.

In accordance with current guidelines, subjects in our amyloid-positive group can be characterized as having preclinical AD (Sperling et al. 2011). The pattern of negative glucose metabolism weights found in the first dimension of the amyloid-positive sparse canonical correlation analysis (see Fig. 2D) closely resembles the known temporoparietal pattern of hypometabolism in AD (Minoshima et al. 1997). This pattern of hypometabolism may be a biomarker of early AD in amyloid-positive cognitively normal older adults. Further, this metabolic pattern was most strongly associated with tau in the medial temporal lobe, where tau initially begins to deposit (Braak and Braak 1991). This suggests that medial temporal lobe tau, generally thought to be associated with aging rather than disease, is not benign when in both high concentrations and in the presence of amyloid-β pathology.

Spatial Associations between Tau and Glucose Metabolism

In cognitively normal older adults, we found that associations between tau and glucose metabolism primarily occurred between distant cortical regions. Our results are consistent with the fact that neurofibrillary tangles are deposited in the somatodendritic compartment of the neuron (Braak and Braak 1991), while glucose metabolism reflects signaling at the synapse (Harris et al. 2012). Long-range projection neurons are also more susceptible to tau pathology than locally projecting neurons (Morrison et al. 1998; Braak et al. 2006), so changes in glucose metabolism in these affected neurons should primarily be found at their downstream projection sites. Previous studies assessing spatial relationships between tau and glucose metabolism within AD patients have generally investigated and observed local associations (Ossenkoppele et al. 2015, 2016; Bischof et al. 2016). However, by the time patient progresses to AD, tau pathology is likely so widespread that distinct spatial patterns with glucose metabolism may be harder to detect.

Our findings support a model in which spatially distinct associations between tau and metabolism reflect the pattern of structural connectivity. Once a sufficient amount of tau is deposited in a region, it seems to affect synaptic function at its downstream sites. For example, in the amyloid-positive group, tau in the entorhinal cortex corresponded with hypometabolism not only locally, but also in regions which receive entorhinal projections, such as the inferior temporal lobe, isthmus cingulate, and orbitofrontal cortex (Canto et al. 2008). Isthmus cingulate tau did not show a strong local effect, however there was a strong negative correlation with orbitofrontal glucose metabolism, reflecting a projection through the cingulum bundle (Mufson and Pandya 1984). Hypometabolism corresponding to structural connectivity is especially interesting because tau is proposed to spread along axonal pathways (De Calignon et al. 2012). These findings are also consistent with previous reports linking hippocampal

atrophy with posterior cingulate cortical hypometabolism (Villain et al. 2008), and with recent reports of tau spreading from the medial temporal lobe to medial parietal cortex via structural connectivity (Jacobs et al. 2018). Therefore, spatially distinct relationships between tau and hypometabolism in cognitively normal older adults may help identify regions that will subsequently develop tau pathology.

The spatial pattern of positive associations between tau and glucose metabolism may also offer insights into the process of tau spread. For example, in the amyloid-negative group, increased tau in the cingulate cortex was associated with greater metabolism in projection sites in frontal cortex. If synaptically driven increased metabolism drives tau spread, one would expect to see tau deposition in the post-synaptic neuron and consequentially local relationships between tau and metabolism in frontal cortex. Longitudinal studies will be necessary to understand these complex relationships.

Limitations

One experimental limitation of this study is the relatively small sample size of the amyloid-positive group combined with the large number of brain regions investigated. We attempted to minimize this problem by using permutation testing to raise confidence in individual correlations, and employing multivariate methods such as the sparse canonical correlation. Therefore, the overall pattern of results should be considered more robust than any specific regional relationship. In addition, because the amyloid-positive group primarily consisted of APOE ε4 positive subjects, we were not able to discriminate between the effects of amyloid-positivity and the effects of APOE ε4 positivity. The amyloid-negative group also demonstrated a significantly higher MMSE score than the amyloid-positive group, with a difference of about a point. It is possible this score difference was associated with our results, reflecting some individuals who are beginning to transition to cognitive decline. While the effects of amyloid-β on cross-sectional measures of cognitive dysfunction in aging are weak, accumulating evidence argues for an effect (Jansen et al. 2018).

Another methodological limitation is the potential for off-target binding of the AV-1451 tracer. Off-target binding has been found to occur in regions such as the choroid plexus (Marquié et al. 2015), which may affect SUVR values in the hippocampus, though other medial temporal regions seem to be spared (Schöll et al. 2016). To raise confidence in our findings, we repeated our major analyses with partial volume corrected data. The partial volume correction method used here (Baker et al. 2017) accounts for spillover from choroid plexus primarily into the hippocampus (Schöll et al. 2016; Baker et al. 2017). Although our major findings are largely consistent with and without PVC, some differences are apparent. While partial volume correction seems to improve signal for AV-1451, these corrections also introduce experimental error. Thus, the application of PVC to our data needs to be interpreted cautiously.

Conclusions

In the present study, we found complex spatial associations between tau and glucose metabolism in cognitively normal older adults that depend on amyloid-β status and the extent of tau pathology in a region. Low levels of tau are associated with increased metabolism that could reflect a benign normal aging process or a substrate for the evolution of neurodegenerative

pathology. High levels of tau, especially in the presence of amyloid-β, are associated with hypometabolism predominantly in spatially distinct regions. Hypometabolism in these regions closely mimics the pattern of temporoparietal hypometabolism found in patients with AD, and may reflect neurodegenerative processes occurring downstream to tau deposition. Longitudinal studies will be necessary to fully characterize the directionality and trajectory of tau's relationship with glucose metabolism in both aging and disease.

Supplementary Material

Supplementary material is available at *Cerebral Cortex* online.

Notes

We thank the members of the Jagust Lab for helpful comments and discussion. *Conflict of Interest*: None declared.

References

Altmann A, Ng B, Landau SM, Jagust WJ, Greicius MD. 2015. Regional brain hypometabolism is unrelated to regional amyloid plaque burden. Brain. 138:3734–3746.

Baker SL, Maass A, Jagust WJ. 2017. Considerations and code for partial volume correcting [18F]-AV-1451 tau PET data. Data Br. 15:648–657.

Bischof N, Jessen F, Fliessbach K, Dronse J, Hammes J. 2016. Impact of tau and amyloid burden on glucose metabolism in Alzheimer's disease. Ann Clin Transl Neurol. 3:934–939.

Braak H, Braak E. 1991. Neuropathological stageing of Alzheimer-related changes. Acta Neuropathol. 82:239–259.

Braak H, Braak E. 1997. Frequency of stages of Alzheimer-related lesions in different age categories. Neurobiol Aging. 18:351–357.

Braak H, Udo R, Schultz C, Del Tredici K. 2006. Vulnerability of cortical neurons to Alzheimer's and Parkinson's diseases. J Alzheimers Dis. 9:35–44.

Brendel M, Probst F, Jaworska A, Overhoff F, Korzhova V, Albert NL, Beck R, Lindner S, Gildehaus F-J, Baumann K, et al. 2016. Glial activation and glucose metabolism in a transgenic amyloid mouse model: a triple-tracer PET study. J Nucl Med. 57:954–960.

Brier MR, Gordon B, Morris JH, Benzinger TLS, Ances BM. 2016. Tau and Aβ imaging, CSF measures, and cognition in Alzheimer's disease. Sci Transl Med. 8:1–10.

Canto CB, Wouterlood FG, Witter MP. 2008. What does the anatomical organization of the entorhinal cortex tell us? Neural Plast. 2008:381243.

Cho H, Choi JY, Hwang MS, Kim YJ, Lee HM, Lee HS, Lee JH, Ryu YH, Lee MS, Lyoo CH. 2016. In vivo cortical spreading pattern of tau and amyloid in the Alzheimer's disease spectrum. Ann Neurol. 80:247–258.

Crary JF, Trojanowski JQ, Schneider JA, Abisambra JF, Abner EL, Alafuzoff I, Arnold SE, Attems J, Beach TG, Bigio EH, et al.

2014. Primary age-related tauopathy (PART): a common pathology associated with human aging. Acta Neuropathol. 128:755–766.

De Calignon A, Polydoro M, Suárez-Calvet M, William C, Adamowicz DH, Kopeikina KJ, Pitstick R, Sahara N, Ashe KH, Carlson GA, et al. 2012. Propagation of tau pathology in a model of early Alzheimer's disease. Neuron. 73:685–697.

Furst AJ, Rabinovici GD, Rostomian AH, Steed T, Alkalay A, Racine C, Miller BL, Jagust WJ. 2012. Cognition, glucose metabolism and amyloid burden in Alzheimer's disease. Neurobiol Aging. 33:215–225.

Hanseeuw BJ, Betensky RA, Schultz AP, Papp KV, Mormino EC, Sepulcre J, Bark JS, Cosio DM, LaPoint M, Chhatwal JP, et al. 2017. Fluorodeoxyglucose metabolism associated with tau-amyloid interaction predicts memory decline. Ann Neurol. 81:583–596.

Harris JJ, Jolivet R, Attwell D. 2012. Synaptic energy use and supply. Neuron. 75:762–777.

Heneka MT, Carson MJ, El Khoury J, Landreth GE, Brosseron F, Feinstein DL, Jacobs AH, Wyss-Coray T, Vitorica J, Ransohoff RM, et al. 2015. Neuroinflammation in Alzheimer's disease. Lancet Neurol. 14:388–405.

Hotelling H. 1936. Relations between two sets of variates. Biometrika. 28:321.

Härdle W, Simar L. 2007. Applied multivariate statistical analysis. Berlin (Germany): Springer.

Jacobs HIL, Hedden T, Schultz AP, Sepulcre J, Perea RD, Amariglio RE, Papp KV, Rentz DM, Sperling RA, Johnson KA. 2018. Structural tract alterations predict down-stream tau accumulation in amyloid positive older individuals. Nat Neurosci. 10.1038/s41593-018-0070-z.

Jagust WJ, Landau SM. 2012. Apolipoprotein E, not fibrillar B-amyloid, reduces cerebral glucose metabolism in normal aging. J Neurosci. 32:18227–18233.

Jansen WJ, Ossenkoppele R, Tijms BM, Fagan AM, Hansson O, Klunk WE, Van Der Flier WM, Villemagne VL, Frisoni GB, Fleisher AS, et al. 2018. Association of cerebral amyloid-β aggregation with cognitive functioning in persons without dementia. JAMA Psychiatry. 75:84–95.

La Joie R, Perrotin A, Barre L, Hommet C, Mezenge F, Ibazizene M, Camus V, Abbas A, Landeau B, Guilloteau D, et al. 2012. Region-specific hierarchy between atrophy, hypometabolism, and β-amyloid (Aβ) load in Alzheimer's Disease dementia. J Neurosci. 32:16265–16273.

LaPoint MR, Chhatwal JP, Sepulcre J, Johnson KA, Sperling RA, Schultz AP. 2017. The association between tau PET and retrospective cortical thinning in clinically normal elderly. NeuroImage. 157:612–622.

Li Y, Rinne JO, Mosconi L, Pirraglia E, Rusinek H, Desanti S, Kemppainen N, Någren K, Kim BC, Tsui W, et al. 2008. Regional analysis of FDG and PIB-PET images in normal aging, mild cognitive impairment, and Alzheimer's disease. Eur J Nucl Med Mol Imaging. 35:2169–2181.

Logan J. 2000. Graphical analysis of PET data applied to reversible and irreversible tracers. Nucl Med Biol. 27:661–670.

Lowe VJ, Weigand SD, Senjem ML, Vemuri P, Jordan L, Kantarci K, Boeve B, Jack CR, Knopman D, Petersen RC. 2014. Association of hypometabolism and amyloid levels in aging, normal subjects. Neurology. 82:1959–1967.

Maass A, Landau S, Baker SL, Horng A, Lockhart SN, La Joie R, Rabinovici GD, Jagust WJ. 2017. Comparison of multiple tau-PET measures as biomarkers in aging and Alzheimer's disease. NeuroImage. 157:448–463.

Maass A, Lockhart SN, Harrison TM, Bell RK, Mellinger T, Swinnerton K, Baker SL, Rabinovici GD, Jagust WJ. 2017. Entorhinal tau pathology, episodic memory decline and neurodegeneration in aging. J Neurosci. 38:530–543.

Marks SM, Lockhart SN, Baker SL, Jagust WJ. 2017. Tau and β-amyloid are associated with medial temporal lobe structure, function and memory encoding in normal aging. J Neurosci. 37:3769–16.

Marquié M, Normandin MD, Vanderburg CR, Costantino IM, Bien EA, Rycyna LG, Klunk WE, Mathis CA, Ikonomovic MD, Debnath ML, et al. 2015. Validating novel tau positron emission tomography tracer [F-18]-AV-1451 (T807) on postmortem brain tissue. Ann Neurol. 78:787–800.

Mathis CA, Wang Y, Holt DP, Huang GF, Debnath ML, Klunk WE. 2003. Synthesis and evaluation of 11C-labeled 6-substituted 2-arylbenzothiazoles as amyloid imaging agents. J Med Chem. 46:2740–2754.

Minoshima S, Giordani B, Berent S, Frey KA, Foster NL, Kuhl DE. 1997. Metabolic reduction in the posterior cingulate cortex in very early Alzheimer's disease. Ann Neurol. 42:85–94.

Mormino EC, Smiljic A, Hayenga AO, Onami SH, Greicius MD, Rabinovici GD, Janabi M, Baker SL, Yen V, Madison I, et al. 2011. Relationships between beta-amyloid and functional connectivity in different components of the default mode network in aging. Cereb Cortex. 21:2399–2407.

Morrison BM, Hof PR, Morrison JH. 1998. Determinants of neuronal vulnerability in neurodegenerative diseases. Ann Neurol. 44:S32–S44.

Mufson EJ, Pandya DN. 1984. Some observations on the course and composition of the cingulum bundle in the rhesus monkey. J Comp Neurol. 225:31–43.

Oh H, Habeck C, Madison C, Jagust W. 2014. Covarying alterations in Aβ deposition, glucose metabolism, and gray matter volume in cognitively normal elderly. Hum Brain Mapp. 35: 297–308.

Ong WY, Tanaka K, Dawe GS, Ittner LM, Farooqui AA. 2013. Slow excitotoxicity in Alzheimer's Disease. J Alzheimer's Dis. 35:643–668.

Ossenkoppele R, Madison C, Oh H, Wirth M, Van Berckel BNM, Jagust WJ. 2014. Is verbal episodic memory in elderly with amyloid deposits preserved through altered neuronal function? Cereb Cortex. 24:2210–2218.

Ossenkoppele R, Schonhaut DR, Baker SL, O'Neil JP, Janabi M, Ghosh PM, Santos M, Miller ZA, Bettcher BM, Gorno-Tempini ML, et al. 2015. Tau, amyloid, and hypometabolism in a patient with posterior cortical atrophy. Ann Neurol. 77:338–342.

Ossenkoppele R, Schonhaut DR, Schöll M, Lockhart SN, Ayakta N, Baker SL, O'Neil JP, Janabi M, Lazaris A, Cantwell A, et al. 2016. Tau PET patterns mirror clinical and neuroanatomical variability in Alzheimer's disease. Brain. 139:1551–1567.

Planel E, Miyasaka T, Launey T, Chui D-H, Tanemura K, Sato S, Murayama O, Ishiguro K, Tatebayashi Y, Takashima A. 2004. Alterations in glucose metabolism induce hypothermia leading to tau hyperphosphorylation through differential inhibition of kinase and phosphatase activities: implications for Alzheimer's disease. J Neurosci. 24:2401–2411.

Price JC, Klunk WE, Lopresti BJ, Lu X, Hoge JA, Ziolko SK, Holt DP, Meltzer CC, DeKosky ST, Mathis CA. 2005. Kinetic modeling of amyloid binding in humans using PET imaging and Pittsburgh Compound-B. J Cereb Blood Flow Metab. 25: 1528–1547.

Rabinovici GD, Furst AJ, Alkalay A, Racine CA, O'Neil JP, Janabi M, Baker SL, Agarwal N, Bonasera SJ, Mormino EC, et al.

2010. Increased metabolic vulnerability in early-onset Alzheimer's disease is not related to amyloid burden. Brain. 133:512–528.

Rocher AB, Chapon F, Blaizot X, Baron JC, Chavoix C. 2003. Resting-state brain glucose utilization as measured by PET is directly related to regional synaptophysin levels: a study in baboons. NeuroImage. 20:1894–1898.

Rousset OG, Ma Y, Evans AC. 1998. Correction for partial volume effects in PET: principle and validation. J Nucl Med. 39: 904–911.

Schultz AP, Chhatwal JP, Hedden T, Mormino EC, Hanseeuw BJ, Sepulcre J, Huijbers W, LaPoint M, Buckley RF, Johnson KA, et al. 2017. Phases of hyper and hypo connectivity in the default mode and salience networks track with amyloid and tau in clinically normal individuals. J Neurosci. 37:4323–4331.

Schöll M, Lockhart SN, Schonhaut DR, O'Neil JP, Janabi M, Ossenkoppele R, Baker SL, Vogel JW, Faria J, Schwimmer HD, et al. 2016. PET imaging of tau deposition in the aging human brain. Neuron. 89:971–982.

Shen X, Liu H, Hu Z, Hu H, Shi P. 2012. The relationship between cerebral glucose metabolism and age: report of a large brain PET data set. PLoS One. 7:e51517.

Sperling RA, Aisen PS, Beckett LA, Bennett DA, Craft S, Fagan AM, Iwatsubo T, Jack CR, Kaye J, Montine TJ, et al. 2011. Toward defining the preclinical stages of Alzheimer's disease: recommendations from the National Institute on Aging-Alzheimer's Association workgroups on diagnostic guidelines for Alzheimer's disease. Alzheimer's Dement. 7:280–292.

Villain N, Desgranges B, Viader F, de la Sayette V, Mezenge F, Landeau B, Baron J-C, Eustache F, Chetelat G. 2008. Relationships between hippocampal atrophy, white matter disruption, and gray matter hypometabolism in Alzheimer's disease. J Neurosci. 28:6174–6181.

Wang Y, Mandelkow E. 2015. Tau in physiology and pathology. Nat Rev Neurosci. 17:22–35.

Witten DM, Tibshirani R, Hastie T. 2009. A penalized matrix decomposition, with applications to sparse principal components and canonical correlation analysis. Biostatistics. 10: 515–534.

Wu JW, Hussaini SA, Bastille IM, Rodriguez GA, Mrejeru A, Rilett K, Sanders DW, Cook C, Fu H, Boonen RACM, et al. 2016. Neuronal activity enhances tau propagation and tau pathology in vivo. Nat Neurosci. 19:1085–1092.

Xia CF, Arteaga J, Chen G, Gangadharmath U, Gomez LF, Kasi D, Lam C, Liang Q, Liu C, Mocharla VP, et al. 2013. [(18)F]T807, a novel tau positron emission tomography imaging agent for Alzheimer's disease. Alzheimers Dement. 9:666–676.

Yi D, Lee DY, Sohn BK, Choe YM, Seo EH, Byun MS, Woo JI. 2014. Beta-amyloid associated differential effects of APOE4 on brain metabolism in cognitively normal elderly. Am J Geriatr Psychiatry. 22:961–970.

Zuendorf G, Kerrouche N, Herholz K, Baron J-C. 2003. Efficient principal component analysis for multivariate 3D voxel-based mapping of brain functional imaging data sets as applied to FDG-PET and normal aging. Hum Brain Mapp. 18: 13–21.